# Pulsed DC magnetron sputtering of transparent conductive oxide layers

**Astrid Bingel[1,2*], Kevin Füchsel[1,2], Norbert Kaiser[2], and Andreas Tünnermann[1,2]**

[1] *Institute of Applied Physics, Abbe Center of Photonics, Friedrich-Schiller-Universität Jena, Max-Wien-Platz 1, 07743 Jena, Germany*

[2] *Fraunhofer Institute for Applied Optics and Precision Engineering, Albert-Einstein-Str. 7, 07745 Jena, Germany*

[*] *Corresponding author: astrid.bingel@uni-jena.de*

Received December 10, 2012; accepted December 26, 2012; posted online May 9, 2013

A comprehensive material study of different transparent conductive oxides (TCOs) is presented. The layers are deposited by pulsed direct current (DC) magnetron sputtering in an inline sputtering system. Indium tin oxide (ITO) films are studied in detail. The optimum pressure of 0.33 Pa (15Ar:2$O_2$) produces a 300-nm thin film with a specific resistivity $\rho$ of $2.2\times10^{-6}$ Ωm and a visual transmittance of 81%. Alternatively, ZnO:Al and ZnO:Ga layers with thicknesses of 200 and 250 nm are deposited with a minimum resistivity of $5.5\times10^{-6}$ and $6.8\times10^{-6}$ Ωm, respectively. To compare the optical properties in the ultraviolet (UV) range, the optical spectra are modeled and the band gap is determined.

*OCIS codes:* 310.0310, 220.0220, 160.0160.

*doi: 10.3788/COL201311.S10201.*

Transparent conductive oxides (TCOs) are used in a wide field of application due to their extraordinary material properties. They combine a metal-like conductivity with a high transparency in the visual spectral range. Therefore they are well-suited for the application as transparent electrodes in organic light-emitting diodes (OLEDs), flat panel displays, and solar cells[1−3]. In the latter case, a promising concept is the semiconductor-insulator-semiconductor (SIS) solar cell[4,5]. Here, the TCO acts as a transparent electrode and simultaneously induces the inversion of the material. Owing to its rectifying properties, SIS devices can be used for light sensors as well.

In general, indium tin oxide (ITO) films provide the best compromise between electrical conductivity and visual transparency. Also, its relatively large band gap might enable sensor applications in the ultraviolet (UV) spectral range. However, the high costs of indium forced the investigation of many kinds of substitutes. A promising candidate is doped zinc oxide, especially ZnO:Al, because the electrical properties are meanwhile comparable to that of ITO but it is nontoxic and cost-saving. Another option is the use of gallium-doped zinc oxide (ZnO:Ga).

To ensure high quality films as well as moderate production costs, inline pulsed direct current (DC) magnetron sputtering is a very good deposition process for producing thin TCO films. This letter presents the electrical, optical, and structural characterization, as well as the individual optimization of different TCO materials. Additionally, simulations of the transmittance and reflectance spectra are carried out to obtain the optical constants that contain information about the band gap of the materials.

The TCO layers were all deposited by pulsed DC magnetron sputtering. The plant that was used is an MRC903 inline sputtering system with a sputter down geometry. The deposition was carried out dynamically meaning that the substrate carrier was moved below the three available target stations with a velocity of approximately 130 cm/min. The film thickness could be varied by the number of passes. The target to substrate distance amounts to 60 mm and the targets have a size of 380×120 (mm). The sputter pulse frequency was kept constant to 100 kHz and the operating power was 1 500 W. Before starting the deposition process, the chamber was evacuated to a base pressure of $9\times10^{-5}$ Pa. The process gases Ar and $O_2$ were inset by mass flow controllers. A direct substrate heating within the sputtering chamber was not available. However, the substrates could be heated within the loadlock of the system by halogen lamps. This provides a rapid annealing for approximately 7 min at temperatures up to 350 °C before and after the deposition.

In this letter, different TCO materials were deposited. ITO was used with a target composition of $In_2O_3$:$SnO_2$ 87:13 wt.-%. The dopant compound in the ZnO:$Al_2O_3$ and ZnO:$Ga_2O_3$ targets was 2 wt.-% $Al_2O_3$ and 6 wt.-% $Ga_2O_3$, respectively.

The electrical film characterization was done by linear four point probe measurements as well as Hall measurements in van-der-Pauw geometry. The optical transmittance and reflectance spectra were recorded using a PerkinElmer Lambda 850 spectrometer. The surface morphology of the films was observed using a "ΣIGMA" (Carl Zeiss) scanning electron microscope (SEM).

In order to achieve maximum efficiency of the optoelectronic devices that contain the TCO layers, it is very important to optimize at first the material itself. For that purpose, ITO films were deposited on 1" glass substrates from a target with a compounding of 87 wt.-% $In_2O_3$ and 13 wt.-% $SnO_2$. The film thickness was kept constant at about 300 nm in order to ensure the comparability of the results, since it is well known that the specific resistivity shows a decrease with film thickness[6]. The sputtering of thin ITO films without substrate heat-

 

ing produces a specific resistivity in the range of about $1.5\times10^{-5}$ Ωm and a relatively low visual transmittance of 80%. These values are far away from the optimum ITO parameters that can be achieved[7] and it is well known that a high quality ITO film requires a higher substrate temperature[8]. Therefore, the further optimization of gas compounding as well as process pressure was done with the presence of substrate heating. As it was described in the experimental section, the sputtering system is not provided with a direct substrate heating. Hence, the halogen lamps within the load lock were used to provide a heat impact into the layer. Directly before and after the deposition, the substrates were heated for 7 min up to a temperature of 350 °C.

The optimum $O_2$ content in the sputter gas was investigated. For that purpose, 300-nm thin ITO layers were deposited with a varying oxygen flow whereas the Ar flow was kept constant at 10 sccm. The total pressure was in the range between 0.2 and 0.23 Pa. Figure 1 presents the specific resistivity $\rho$ as well as the carrier concentration $N$ and mobility $\mu$ in dependence of the $O_2$ flow.

As it can be seen, the $O_2$ content in the sputter gas has a great influence on the electrical properties of the ITO layers. Whereas a slight decrease of the specific resistivity from $3\times10^{-6}$ to $2.3\times10^{-6}$ Ωm is achieved by increasing the $O_2$ flow from 1 to 2 sccm, an $O_2$ flow of 3 sccm causes a dramatic rise of $\rho$ to $1.5\times10^{-5}$ Ωm. The origin for this behavior can partly be understood when regarding the carrier concentration and mobility. While $N$ shows a continuous decrease with increasing $O_2$ flow, the mobility has its maximum at 2 sccm. A possible explanation could be the change in stoichiometry if the $O_2$ content in the sputter gas varies. Initially, the stoichiometry is optimized when the flow is increased from 1 to 2 sccm. This leads to fewer defects that could cause electron scattering and therefore the mobility rises from 15 to 31 $cm^2/Vs$. However, if the $O_2$ content in the sputter gas is too high, the mobility is lowered to 23 $cm^2/Vs$. This may be explained by oxygen incorporation into the lattice or segregation of oxygen and Sn to grain boundaries that act as scattering centers for electrons[9]. At the same time, the carrier density drops to $1.5\times10^{20}$ $cm^{-3}$. Additionally, the contribution of oxygen vacancies to the carrier density is reduced if the sputtering is carried out with too much oxygen. The described variations can also be observed in the optical spectra of different layers that can be seen in Fig. 2.

In principal, TCO layers show three characteristic regions in the transmittance and reflectance spectra. Whereas the UV is affected by the bandgap absorption,

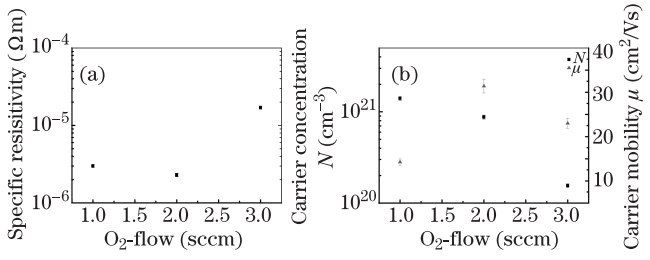


Fig. 1. (a) Specific resistivity $\rho$ as well as (b) the carrier concentration $N$ and mobility $\mu$ of ITO films in dependence of the $O_2$ flow. The Ar flow is kept constant at 10 sccm.

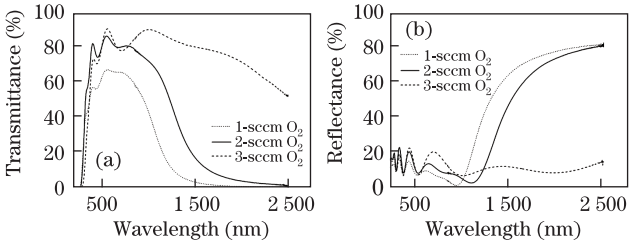


Fig. 2. (a) Transmittance and (b) reflectance spectra of ITO films prepared at different $O_2$ flows. The Ar flow is held constant at 10 sccm.

the visual spectral range shows a high transmittance with the typical Fabry-Perot interferences. Due to the metal-like behavior, high free carrier absorption occurs in the near infrared (NIR) that is followed by a high reflecting region.

The carrier concentration and the free carrier plasma resonance are linked via

$$\omega_{\mathrm{p}}^2 = \frac{Ne^2}{\varepsilon_0 m^*}, \tag{1}$$

where $m^*$ denotes the effectice mass of the material, and $e$ and $\varepsilon_0$ have their usual physical meaning. The optical spectra reflect exactly the change of the carrier concentration displayed in Fig. 1(b). As described above, the carrier concentration decreases with increasing $O_2$ flow. At the same time, both the absorbing region and the change over from high-transmittance to high-reflectance exhibit a red-shift (according to Eq. (1)). For the layer prepared with 3-sccm $O_2$ flow, the carrier concentration amounts to just $1.5\times10^{20}$ $cm^{-3}$, so the high-reflecting region is not even located within the measured spectral range. Additionally, the averaged transmittance in the visual spectral range changes dramatically. The understoichiometric layer prepared with 1-sccm $O_2$ shows just 64% visual transmittance $T_{\mathrm{VIS}}$ in the wavelength range between 400 and 800 nm. As soon as the $O_2$ flow is rised to 2 sccm, the transmittance $T_{\mathrm{VIS}}$ reaches 81.5% and nearly remains constant for 3-sccm $O_2$ flow.

To investigate the structural changes with varying $O_2$ flow, SEM images are shown in Fig. 3.

In general, all films exhibit a columnar structure, but with different characteristics. Whereas the film deposited with 1-sccm $O_2$ shows a surface with nearly round grains, the 2-sccm $O_2$ layer has a three cornered or pyramidal-like surface structure. This forms out more clearly and sharply when increasing the $O_2$ flow to 3 sccm. Apparently, the $O_2$ content during sputtering has a great influence on the microstructure and surface morphology.

After identifying the optimum $O_2$ flow of 2 sccm, also the Ar flow was varied between 7 and 20 sccm, corresponding to a pressure of 0.12–0.47 Pa. Again, the electrical parameters are diagrammed (Fig. 4).

The specific resistivity shows an optimum of $2.2\times10^{-6}$ Ωm at a gas compounding of 15-sccm Ar/2-sccm $O_2$. However, there is no significant change in $\rho$ above an Ar flow of 10 sccm. The transport parameters $N$ and $\mu$ show an opposite behavior. While the carrier concentration rises steadily with increasing Ar flow, the mobility shows a decrease. Here, it is reasonable that the ionized

impurity scattering is the origin for the decrease in $\mu$ for high Ar flows since the carrier concentration is as high as $1\times10^{21}$ cm$^{-3}$.

Again, the variations in the electrical parameters are reflected in the optical spectra (Fig. 5). The plasma absorption shifts to shorter wavelengths with increasing carrier concentration or increasing Ar flow, respectively. Although the film prepared at 20-sccm Ar / 2-sccm $O_2$ exhibits the highest carrier concentration, the resulting conductivity is worse since the mobility is lowered. The visual transmittance shows also its optimum where the resistivty is minimal, namely with 81% nearly the same

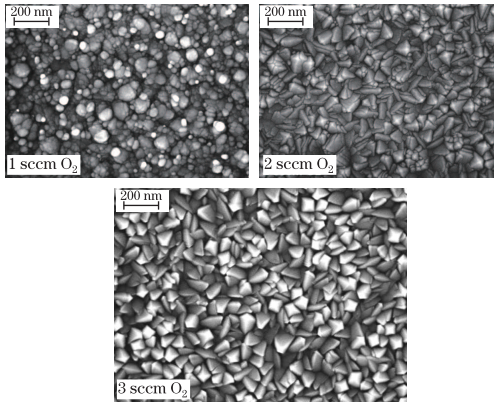


Fig. 3. SEM images of ITO films prepared at different $O_2$ flows. The Ar flow was held constant at 10 sccm.

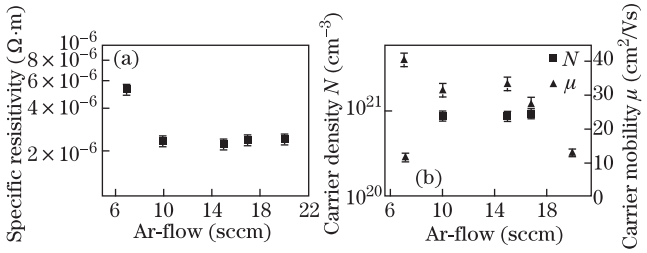


Fig. 4. (a) Specific resistivity as well as (b) the carrier concentration $N$ and mobility $\mu$ of ITO films in dependence of the Ar flow. The $O_2$ flow was kept constant (2 sccm).

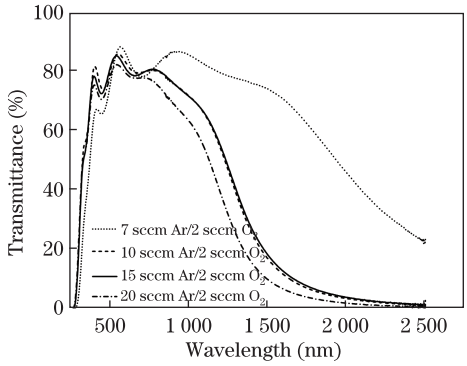


Fig. 5. Transmittance spectra of ITO films prepared at different Ar flows, whereas the $O_2$ flow was kept constant (2 sccm).

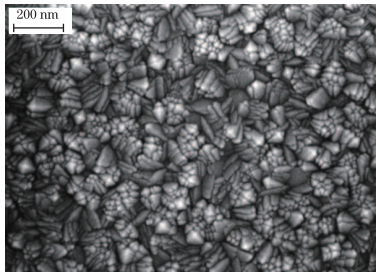


Fig. 6. SEM image of a thin ITO film prepared at optimum sputter gas composition (15-sccm Ar / 2-sccm $O_2$).

value as the 10-sccm Ar / 2-sccm $O_2$ layer. This corresponds to a thickness-independent mean visual extinction value $k$ of about $k_{VIS} = 1.1\times10^{-2}$. However, the transmittance of the films prepared at higher pressure is with 78–79% slightly lower.

To complete the material optimization, Fig. 6 shows the SEM image for the ITO film prepared under optimum deposition conditions.

This microstructure also slightly differs from the others that were observed in Fig. 3. However, we observed this fracture-block-like structure already in earlier studies as the typical ITO structure for an optimum film-conductivity.

Although ITO provides the best conductivity of all known TCO layers, also alternative materials were investigated since indium is nowadays verycost-intensive[10].

A very promising candidate is ZnO:Al which can reach excellent material properties, too and additionally is much more inexpensive. In this study, we only present the results of our material optimization. The optimum target composition was found to be ZnO:$Al_2O_3$ 98:2 wt.-%. This was both published in Ref. [11] and proved by own experiments with different ZnO:$Al_2O_3$ targets. With the same heating procedure as described above and a process pressure of 1.1 Pa (pure Ar), 200-nm thin ZnO:Al films were deposited. A minimum resistivity of $5.5\times10^{-6}$ Ωm could be reached with a corresponding carrier concentration and mobility of $6.1\times10^{20}$ cm$^{-3}$ and 18.4 cm$^2$/Vs, respectively. The mean visual transmittance is with a value of 86.3% ($k_{VIS} = 5\times10^{-3}$) higher than that of the optimum ITO films. This difference is mainly caused by the higher carrier concentration and the accompanying NIR free carrier absorption of the ITO film. This absorption tail also extends to the visual spectral range and therefore raises the value of $k_{VIS}$.

Furthermore, ZnO:Ga was studied with the intention of reaching higher carrier concentration and therefore a larger bandgap[12]. The target composition was chosen to ZnO:$Ga_2O_3$ 94:6 wt.-% and the optimum Ar pressure was in the range of 0.23 Pa. However, contrary to the expectations, the carrier density only amounts to $4.4\times10^{20}$ cm$^{-3}$, whereas the mobility is with 20.8 cm$^2$/Vs slightly higher than that of the ZnO:Al layer. This leads to a specific resistivity of $6.8\times10^{-6}$ Ωm. The extinction coefficient in the visual spectral range is $4.4\times10^{-3}$ that corresponds to a transmittance of 85.6% in a 250-nm thin layer.

The morphology of the ZnO:Al and ZnO:Ga films are

**Table 1. Electrical and Optical Parameters of the Optimized TCO Layers Investigated in This Letter**

| | $\rho$ ($\times 10^{-6}$ Ωm) | $N$ ($\times 10^{20}$cm$^{-3}$) | $\mu$ (cm$^2$/Vs) | $d$ (nm) | $T_{\mathrm{VIS}}$ | $k_{\mathrm{VIS}}$ |
|---|---|---|---|---|---|---|
| ITO | 2.2 | 8.6 | 33.3 | 300 | 81% | $1.1\times10^{-2}$ |
| ZnO:Al | 5.5 | 6.1 | 18.4 | 200 | 86.3% | $5\times10^{-3}$ |
| ZnO:Ga | 6.8 | 4.4 | 20.8 | 250 | 85.6% | $4.4\times10^{-3}$ |

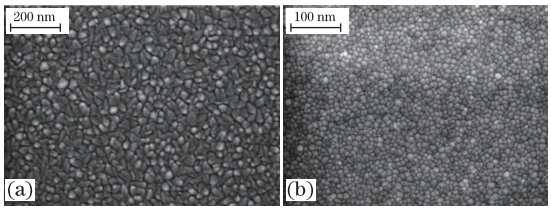


Fig. 7. SEM images of optimized (a) ZnO:Al and (b) ZnO:Ga films.

quite similar (Fig. 7) while a difference to the ITO structure is obvious.

Also this structure shows the top view of a columnar growth. The grains appear not that triangular as it was observed for the optimum ITO films but appear more round in the cross section. A main difference is the grain size that is much smaller than in the ITO films. This is most likely the reason for the significant lower mobility of the ZnO layers.

For a summary, Table 1 shows a comparison of the three materials that were investigated with its most important characteristic parameters.

The optical spectra of thin TCO films contain a lot of information about their band structure as well as their electrical properties. Therefore, it is very enlightening to determine the dielectric function from the optical spectra for a following analysis of the band gap of the material or information about the electrical parameters that are enclosed in the optical spectra.

Since the optical spectra of TCO films are divided into three parts, different approaches for the dielectric functio $\varepsilon$ for the different spectral ranges (e.g., Drude model for the IR, Lorentz oscillator for the UV) would be necessary[13]. However, due to the similarity of the models, in this study we use only one multi-oscillator model to fit the transmittance and reflectance spectra[14],

$$\epsilon = 1 + \frac{1}{\pi}\sum_j J_j\Big(\frac{1}{\nu_{0j} - \nu - i\Gamma_j} + \frac{1}{\nu_{0j} + \nu + i\Gamma_j}\Big), \quad (2)$$

where the parameters $\nu$ and $\nu_0$ represent the wavenumber and resonance wavenumber, respectively. Additionally, the resonance is characterized by the line width of the related absorption $\Gamma_j$ and the intensity factor $J_j$ of the individual harmonic oscillators. With this method, the dispersion including the absorption in the UV as well as the IR is modeled by a superposition of multiple oscillators meaning that arbitrary complex absorption structures are modeled by a defined number of substitutional oscillators[14]. As a result, one can obtain the real and imaginary part of the dielectric function or the optical constants $n$ and $k$ versus the wavelength, respectively. However, the physical meaning of the determined oscillator parameters is not verified. Therefore, further investigations are necessary to obtain, for example, the band gap of the material. Since the investigated materials $In_2O_3$ and ZnO are direct semiconductors[15,16], the optical bandgap can be determined by diagramming the square of the absorption coefficient $\alpha^2$ versus photon energy $E$[17]. The intercept of the linear part of the dielectric function in the UV range with the energy axis can be considered as the band gap $E_g$. Figure 8 shows an example for the determination of $E_g$ of ITO films with different carrier concentrations that are presented before.

After analyzing all samples that were deposited, we obtain a carrier concentration dependent band gap (Fig. 9).

This behavior is well known for TCO materials and caused by the Moss-Burstein effect[18,19]. Due to the high doping of TCOs, the semiconductor becomes degenerated and the Fermi level shifts into the conduction band wherefore the lower states are occupied. Therefore,

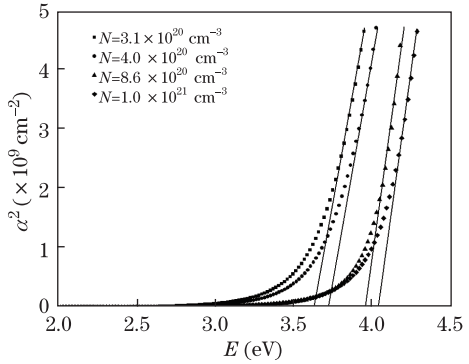


Fig. 8. Determination of the optical band gap $E_g$ for ITO layers with different carrier concentrations. $E_g$ is defined as the intercept of the energy axis that is drawn from the linear part of the $\alpha^2$ function.

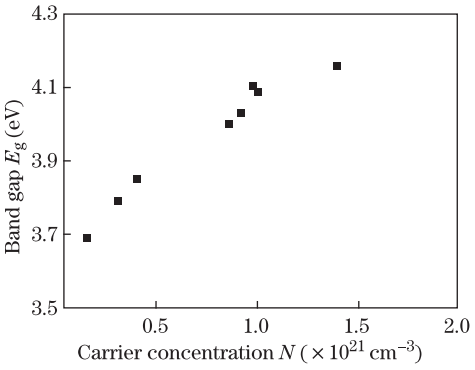


Fig. 9. Optical band gap versus carrier concentration for ITO films.

**Table 2. Optical Properties as well as Carrier Concentration for ITO, ZnO:Al and ZnO:Ga Films Prepared in This Letter**

| Material | ITO | ZnO:Al | ZnO:Ga |
|---|---|---|---|
| Band Gap $E_g$ (eV) | 4.1 | 3.76 | 3.66 |
| $\lambda$ ($T$=50%) (nm) | 332 | 348 | 350 |
| $N$ ($\times 10^{20}$ cm$^{-3}$) | 10.0 | 6.1 | 4.4 |

electrons that are excited from the valence band to the conduction band have to overcome a larger energy gap. As it can be seen in Fig. 9, the band gap rises with increasing carrier concentration since the Fermi level shifts to higher values. The theoretical relationship is given by

$$E_g = E_{g0} + \frac{\hbar^2}{2m^*} \cdot (3\pi^2 N)^{2/3}, \quad (3)$$

whereas $E_{g0}$ denotes the bandgap of an undoped material and $m^*$ is the effective mass. If we now compare all three materials that are investigated in this study, slight differences in the UV can be observed. Table 2 summarizes the band gap analyzation and the corresponding information for ITO, ZnO:Al, and ZnO:Ga layers with the highest carrier concentration.

In principal, ITO shows a higher band gap than ZnO. This is caused by the material itself and is consistent with the theoretical values ($E_{g,\mathrm{ZnO}} = 3.38$ eV[20], $E_{g,\ \mathrm{In_2O_3}}$=3.75 eV[15]). Therefore, ITO has a transparency above 50% down to 332 nm. ZnO:Al and ZnO:Ga hit the 50%-transmission value already at 348 and 350 nm, respectively. This slight difference is caused by the carrier concentration. ZnO:Al exhibits a higher carrier concentration and the corresponding blue shift of the band gap (Moss-Burstein-Shift) is therefore stronger than in ZnO:Ga.

In conclusion, three different TCO materials are studied. The optimization of ITO films is presented in detail. With an optimum sputter gas composition of 15-sccm Ar : 2-sccm $O_2$, a specific resistivity of $2.2\times10^{-6}$ Ωm can be reached. The transmittance in the visual spectral range amounts to 81%. The structure of the films exhibits a significant change by changing the gas composition (SEM). Additionally, a cost-saving alternative to ITO, namely ZnO, is investigated in two variations. Optimized ZnO:Al films exhibits a specific resistivity of $5.5\times10^{-6}$ Ωm whereas the ZnO:Ga films have a slightly higher resistivity $\rho = 6.8\times10^{-6}$ Ωm. This is mainly caused by the lower carrier concentration in ZnO:Ga films. In general, the ZnO films show a lower conductivity due to both a lower carrier concentration and mobility. The latter can be caused by the much smaller grain size of the ZnO films. To investigate the optical properties in the UV spectral range, the transmittance and reflectance spectra are modeled using a multi-oscillator model. As a result, the band gap of the materials can be determined. ITO shows the largest band gap of 4.1 eV. The gap of ZnO:Al and ZnO:Ga are determined to 3.76 and 3.66 eV, respectively. This is originated both in the material itself as well as the lower carrier concentration and therefore weaker Moss-Burstein shift.

This work was supported by the "Novel-Optics" and "ForMaT" Funding Program of the German Federal Ministry of Education and Research under Grant Nos. 13N9669 and 03FO3292.

## References

1. H. Kim, J. S. Horwitz, W. H. Kim, A. J. Mäkinen, Z. H. Kafafi, and D. B. Chrisey, Thin Solid Films **420-421,** 539 (2002).
2. M. Katayama, Thin Solid Films **341,** 140 (1999).
3. J. Müller, O. Kluth, S. Wieder, H. Siekmann, G. Schöpe, W. Reetz, O. Vetterl, D. Lundszien, A. Lambertz, F. Finger, B. Rech, and H. Wagner, Sol. Energ. Mat. Sol. C. **66,** 275 (2001).
4. J. Shewchun, D. Burk, and M. Spitzer, IEEE Trans. Electron. Dev. **27,** 705 (1980).
5. K. Füchsel, A. Bingel, N. Kaiser, and A. Tünnermann, Proc. SPIE **8065,** 80650B (2011).
6. L. Hao, X. Diao, H. Xu, B. Gu, and T. Wang, Appl. Surf. Sci. **254,** 3504 (2008).
7. C. G. Granqvist and A. Hultaker, Thin Solid Films **411,** 1 (2002).
8. H. Kim and C. M. Gilmore, J. Appl. Phys. **86,** 6451 (1999).
9. D. Mergel, W. Stass, G. Ehl, and D. Barthel, J. Appl. Phys. **88,** 2437 (2000).
10. U. S. Geological Survey, "Indium–Statistics and Information", http://minerals.usgs.gov/minerals/pubs/commodity/indium/ (October 11, 2012).
11. C. Agashe, O. Kluth, G. Schöpe, H. Siekmann, J. Hüpkes, and B. Rech, Thin Solid Films **442,** 167 (2003).
12. J. Zhao, X. W. Sun, and S. T. Tan, IEEE Trans. Electron. Dev. **56,** 2995 (2009).
13. Z.-C. Jin, I. Hamberg, and C. G. Granqvist, J. Appl. Phys. **64,** 5117 (2008).
14. O. Stenzel, S. Wilbrandt, K. Friedrich, and N. Kaiser, Vak. Forsch. Prax. **21,** 15 (2009).
15. I. Hamberg and C. G. Granqvist, J. Appl. Phys. **60,** R123 (1986).
16. K. Ellmer, J. Phys. D: Appl. Phys. **34,** 3097 (2001).
17. F. Wooten, *Optical Properties of Solids* (Academic Press, Waltham, 1972).
18. E. Burstein, Phys. Rev. **93,** 632 (1954).
19. T. S. Moss, Proc. Phys. Soc. B **67,** 775 (1954).
20. W. Martienssen and H. Warlimont, *Springer Handbook of Condensed Matter and Materials Data* (Springer, Berlin, 2005).